# Blood Flow Prediction and Visualization within the Aneurysm of the Middle Cerebral Artery after Surgical Treatment

Artem M. Yatchenko[1], Andrey V. Gavrilov[1], Elena V. Boldyreva[2], Ivan V. Arkhipov[3], Elena V. Grigorieva[4], Ivan M. Godkov[4] and Vladimir V. Krylov[4]

[1]*Lomonosov Moscow State University, Moscow, Russia*

[2]*Institute of Machines Science named after A. A. Blagonravov of the Russian Academy of Sciences, Moscow, Russia*

[3]*Petrovsky National Research Center of Surgery of Russian Academy of Medical Sciences, Moscow, Russia*

[4]*Scientific Research Institute of Emergency Care n.a. N. V. Sklifosovsky, Moscow, Russia*

Keywords: Blood Flow, Mathematical Modelling, Computational Fluid Dynamics, Medical Imaging, Neurology.

Abstract: All cerebral aneurysms have the potential to rupture and cause bleeding within the brain. To understand the tactics of treatment of patients with intracranial aneurysms, it is necessary to study in detail the pressure and flow within the aneurysm and vessels. Numerical modelling is a powerful tool for blood flow study, prediction and visualisation. In this paper the method that uses patient-oriented physiological model to determine the numerical modelling parameters is proposed. The experiments were carried out on the real geometry of the patient with two aneurisms of the middle cerebral artery and showed that the proposed methods improves the quality of the surgical planning.

## 1 INTRODUCTION

An aneurysm is a localized, blood-filled balloon-like bulge in the wall of a blood vessel. The rupture of intracranial aneurysm is responsible for 50-70% of all non-traumatic subarachnoid hemorrhage, which may be fatal for the patient in first 2-3 weeks after the accident and lead to disability in about 20-30% of cases (Krylov, Godkov 2011a,b). The risk of recurrent aneurysm's rupture during the first 2 weeks is up to 20% and during the first 6 months is up to 50%. The morbidity rate for re-rupture of the aneurysm reaches to 68-70%.

The surgery approaches in patients with intracranial aneurysms primarily due to its structure and related hemodynamic disorders, both in parent vessels of aneurysm and in the arterial circle of the brain in whole. The results of several recent studies show that the risk factors of aneurysm's rupture and re-rupture include not only its size, location and other features, but also different hemodynamic changes in the parent artery (Krylov et al, 2013a, Chupakin and Cherevko, 2012, Sforza et al, 2009, Tateshima et al, 2007). For example, D. Sforza et al. (2009) believes that the major role in the growth and subsequent rupture plays so called "environment" of aneurysm, referring primarily to the related changes of brain arteries. At the same time the average age of patients with aneurysmal rupture ranges from 40 to 60 years and accompanied with atherosclerosis and other disorders of intracranial arteries. So as it is necessary to investigate the dependence of associated hemodynamic changes in parent artery and its branches, first of all due to atherosclerotic stenosis and occlusions (Krylov and Godkov 2011b).

Numerical modelling provide great opportunities for blood flow study and is widely used in modern scientific research (Watton et al, 2011, Olufsen et al, 2000, Kim et al, 2010, Krylov et al, 2013a). The most difficult part is setting the boundary conditions on the ends of the vessels. The study of resistance of vessel systems is used for these purposes. The resistance of invisible part (peripheral resistance) plays the crucial role in flow definition. To estimate the peripheral resistances statistical (Kim et al, 2010) and fractal (Olufsen et al, 2000) models are used.

In this work to determine the parameters of the vessels and the peripheral resistances the method that uses patient-oriented physiological model and geometry analysis is proposed.



Yatchenko A., Gavrilov A., Boldyreva E., Arkhipov I., Grigorieva E., Godkov I. and Krylov V..
Blood Flow Prediction and Visualization within the Aneurysm of the Middle Cerebral Artery after Surgical Treatment.
DOI: 10.5220/0005461301080113
In *Proceedings of the 5th International Workshop on Image Mining. Theory and Applications* (IMTA-5-2015), pages 108-113
ISBN: 978-989-758-094-9

## 2 ANATOMICAL GEOMETRY RECONSTRUCTION

A series of 661 CT images with resolution 512x512 of a real patient with 2 aneurisms of the middle cerebral artery was used as input data for further processing. A pixel spacing of the CT slices is 0.45 mm, a distance between slices is 0.35 mm. This resolution is sufficient for large vessels representation with diameter 1–2 mm, but small vessels with diameter less than 1 mm are barely distinguishable. A direct volume visualization of a vessel of interest is shown in figure 1(a).

The Marching-cubes algorithm (Lorensen and Cline, 1987) was used for inner vessel surface reconstruction as a CT haunsfield isosurface. A resulting polygonal mesh was further converted into a set of parametric surfaces. This is a common way for setting a geometry for Computer-Aided Design (CAD) systems (see fig. 1(b)).

All parts of the vessels and two aneurisms were labelled and numbered, and the final scheme of the investigated system is shown in figure 2. The arrow indicates the direction of blood flow.

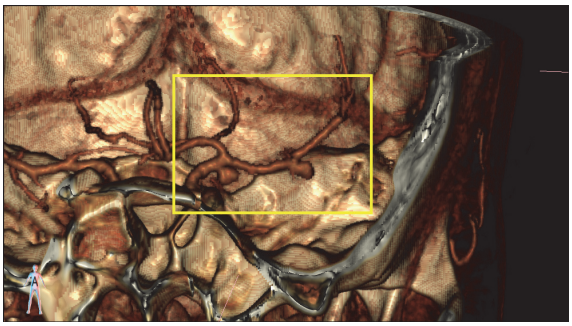

(a)

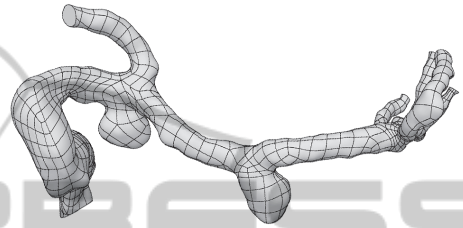

(b)

Figure 1: (a) anatomical direct volume visualization of the described vessel system, (b) CAD geometry representation of the system.

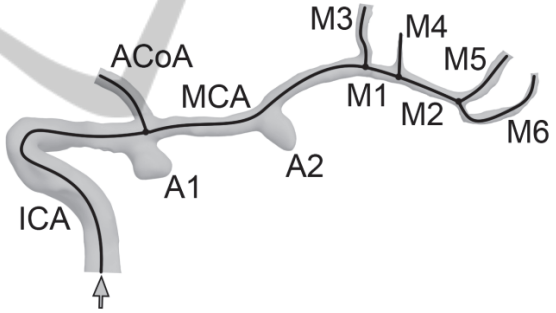


Figure 2: Scheme of the vessels (ICA – Internal Carotid Artery, ACoA – Anterior Communicative Artery, MCA – Middle Cerebral Artery) and aneurisms (A1 and A2).

## 3 VESSEL PARAMETERS DETECTION

For each straight vessel $\alpha$ of the system volume $V_\alpha$ and lateral surface area $S_\alpha$ were determined. Imagining the vessel as a cylinder with radius $r_\alpha$ and length $l_\alpha$ and representing $V_\alpha$ and $S_\alpha$ as

$$V_\alpha = \pi {r_\alpha}^2 l_\alpha, \quad S_\alpha = 2\pi r_\alpha l_\alpha, \tag{1}$$

we will get

$$r_\alpha = \frac{2V_\alpha}{S_\alpha}, \qquad l_\alpha = \frac{{S_\alpha}^2}{4\pi V_\alpha}. \tag{2}$$

Obtained length and radius of each vessel are listed in table 1.

Table 1: Obtained geometric parameters (length and radius) of the vessels.

| Vessel | ICA | MCA | M1 | M2 | ACoA | M3 | M4 | M5 | M6 |
|---|---|---|---|---|---|---|---|---|---|
| Length [mm] | 40.5 | 32.6 | 9.48 | 8.8 | 11.5 | 14.1 | 5.09 | 9 | 11.5 |
| Radius [mm] | 1.98 | 1.15 | 0.91 | 0.96 | 1.09 | 0.83 | 0.58 | 0.84 | 0.64 |

Resistance of a vessel is a number $R$ that characterizes the dependence of a pressure drop $\Delta P$ at ends of the vessel on a constant volume flow $Q$:

$$R = \frac{\Delta P}{Q}. \tag{3}$$

The resistance of a vessel system can be calculated similarly to the electrical circuit schemas using formulas (4) for series and parallel connection of vessels.

$$R_{series} = R_1 + R_2, \ \frac{1}{R_{parallel}} = \frac{1}{R_1} + \frac{1}{R_2}. \tag{4}$$

For laminar flows the resistance of a vessel does not depend on the flow $Q$ and can be calculated using the vessel geometry and the liquid parameters.

In our calculations two methods were tested for resistance estimation:

- Poiseuille equation;
- Numerical experiment.

### 3.1 Poiseuille Equation

In fluid dynamics the Hagen–Poiseuille law is a physical law that gives the pressure drop in a fluid flowing through a long cylindrical pipe:

$$\Delta P = \frac{8\eta l Q}{\pi r^4}, \quad (5)$$

where $\Delta P$ is the pressure drop, $l$ is the length of pipe, $\eta$ is the dynamic viscosity of liquid, $Q$ is the volumetric flow rate and $r$ is the radius.

Thus, the resistance of a vessel can be calculated using the following equation:

$$R = \frac{\Delta P}{Q} = \frac{8\eta l}{\pi r^4}. \quad (6)$$

### 3.2 Numerical Experiment

For the vessel resistance measurement Reynolds-Averaged Navier-Stokes equations can be used.

A constant flow nave been simulated through each vessel and a pressure drop was measured. The geometry of a vessel was fragmented into the mesh of finite elements. The approximate size of elements was selected 0.2 mm. The selection of element size is described in the next section. The mesh is more fine near the wall of a vessel to provide better fluid-wall interaction (see figure 3). ANSYS CFX 15.0 was used for computation task.

The blood was set as a Nuewton liquid with density $\rho = 1080$ [kg/m$^3$] and viscosity $\eta = 0.00388$ [Pa·s]. These parameters correspond to normal blood parameters (Brown et al, 2013). Volumetric flow $Q$ is 10 [mm$^3$/s].

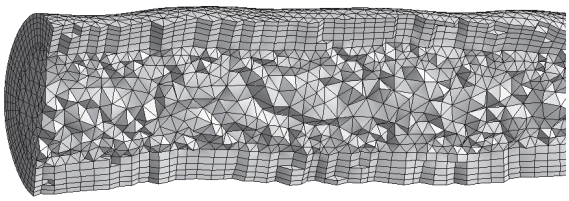

Figure 3: Adjacent layer of the mesh.

The results of resistance measurement via Hagen–Poiseuille equation and the numerical experiment are shown in table 2.

Table 2: Resistance of the vessels measurement detected via Hagen–Poiseuille equation (R, Poiseuille) and the numerical experiment (R, ANSYS).

| Vessel | ICA | MCA | M1 | M2 | ACoA |
|---|---|---|---|---|---|
| R, Poiseuille [Pa·s/mm$^3$] | 0.026 | 0.187 | 0.138 | 0.103 | 0.081 |
| R, ANSYS [Pa·s/mm$^3$] | 0.128 | 0.249 | 0.06 | 0.151 | 0.235 |
| Vessel | M3 | M4 | M5 | M6 | |
| R, Poiseuille [Pa·s/mm$^3$] | 0.296 | 0.443 | 0.177 | 0.663 | |
| R, ANSYS [Pa·s/mm$^3$] | 0.783 | 1.483 | 0.196 | 1.812 | |

## 4 ELEMENT SIZE SELECTION

To determine the optimal size of finite elements to use in the computational experiments for vessel resistance estimation real vessel geometry was used (see fig. 4 (a)). The resistance of this vessel was calculated using Hagen–Poiseuille Equation and using numerical flow computation with different element sizes.

To make the Hagen–Poiseuille equation result more accurate the vessel was fragmented at 15 parts (see fig. 4 (b)). Radius and length of each part were determined and a resistance of each part was computed. The total resistance of the vessel was calculated as a resistance of a series connection of several vessels.

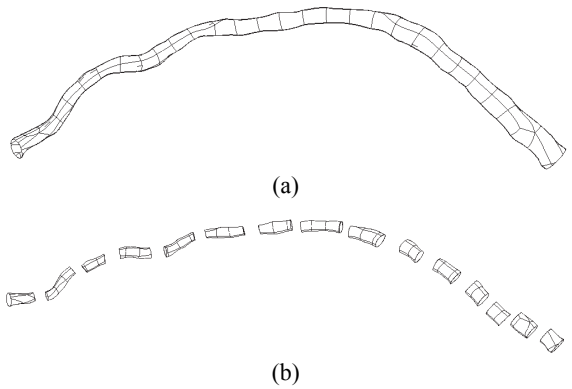

(a)

(b)

Figure 4: (a) The geometry of the examined vessel and (b) its fragmentation on 15 parts.

Finite element meshes with different element size were tested. The element size was 1 mm, 0.7 mm, 0.3 mm, 0.2 mm, 0.1 mm, 0.08 mm and 0.05 mm with total number of elements 7530, 12947, 57365, 136550, 627121, 1028359 and 2895589 respectively. Examples of some meshes are presented in figure 5.

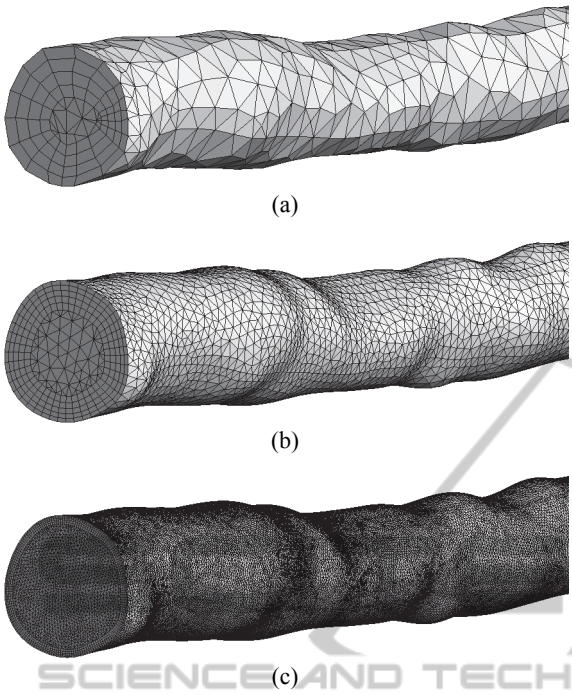

Figure 5: The finite elements mesh: (a) 7530 elements, (b) 57365 elements, (c) 1028359 elements.

To produce distinctly laminar flow the volumetric flow $Q = 10$ mm$^3$/s was simulated.

The results of obtained resistance and computation time are in table 3.

Table 3: Obtained resistance of the vessel.

| Element size, [mm] | Elements count | $\Delta P$, [Pa] | R, [Pa·s/mm$^3$] | Computation Time |
|---|---|---|---|---|
| 1 | 7 530 | 1101.6 | 2.35 | 17 s |
| 0.7 | 12 947 | 1181.96 | 2.53 | 14 s |
| 0.3 | 57 365 | 1033 | 2.21 | 23 s |
| 0.2 | 136 550 | 1030.12 | 2.2 | 38 s |
| 0.1 | 627 121 | 1016.49 | 2.17 | 3 min 10 s |
| 0.08 | 1 028 359 | 1012.82 | 2.17 | 6 min 13 s |
| 0.05 | 2 895 589 | 1011.55 | 2.16 | 7 min 42 s |

It can be seen that approximately 150 thousands elements give an appropriate accuracy of measurement with relatively low computation time costs.

## 5 PHYSIOLOGICAL MODEL

There have been numerous theoretical attempts to explain the design of vascular trees based on the principles of minimum work (Murray, 1926a,b, Oka, 1974), optimal design (Rosen, 1967), minimum blood volume (Kamiya and Togawa, 1972) and minimum total shear force on the vessel wall (Zamir, 1976, 1977). These attempts have resulted in relationships between the geometry and flow parameters of the mother and daughter vessels at a bifurcation.

Figure 6 shows the relationship between normalized flow through a vessel segment and normalized segment diameter for the arterial tree, excluding the capillaries. This is an isodensity plot showing five layers of frequency. As expected, the majority of vessels are the smaller-diameter arterioles. The diameter and flow are normalized with respect to the inlet, most proximal segment. The relationship obeys a power law relation as suggested by Murray's law. However, the value of exponent is not 3, as predicted by Murray's law. As determined by least-squares fits of the data, the exponent has values of 2.2, 2.1 and 2.1 for RCA, LAD, and LCx, respectively (Mittal et al, 2005).

In our calculations we assume that volumetric flow in daughter vessels at a bifurcation be calculated using the following equations:

$$Q_1 = \frac{Q{d_1}^{2.2}}{{d_1}^{2.2} + {d_2}^{2.2}} = \frac{Q{S_1}^{1.1}}{{S_1}^{1.1} + {S_2}^{1.1}},$$
$$Q_2 = \frac{Q{d_2}^{2.2}}{{d_1}^{2.2} + {d_2}^{2.2}} = \frac{Q{S_2}^{1.1}}{{S_1}^{1.1} + {S_2}^{1.1}}, \quad (7)$$

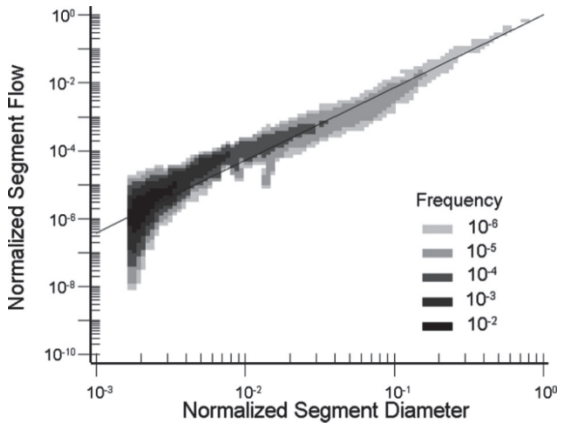


Figure 6: An isodensity plot showing 5 layers of frequency between normalized stem flow and normalized diameter of the stem for the left anterior descending coronary artery (LAD) arterial tree.

where $Q$ is a volumetric flow in mother vessel, $Q_1$ and $Q_2$ are flows in daughter vessels, $d_1$ and $d_2$ are diameters of daughter vessels and $S_1$ and $S_2$ are

cross-section areas.

The flow in the ICA was taken from tables $Q_0 = 2.5ml/s = 2500mm^3/s$. Using (5) and the data from table 1 the flow in all parts of investigated vessel system has been calculated.

After the volumetric flows in all considered vessels are determined the numerical calculation can be performed. The pressure in ICA was set 13000 Pa. The pressure in capillaries was set 3000 Pa. The laminar steady flow model was used.

The total pressure drop from ICA to capillaries occurs in investigated visible vessels and in invisible vessels (too small for CT or MRI scanning). The resistance of invisible part of a system is a peripheral resistance. The peripheral resistance is a crucial value in flow prediction and can be calculated as

$$R_p = \frac{P_{end} - P_{capillary}}{Q}. \quad (8)$$

The results of volumetric flow in the vessels and peripheral resistances calculation are in table 4. The pressure in aneurisms A1 and A2 was determined 11104 Pa and 10230 Pa.

Table 4: A volumetric flow through the vessels; peripheral resistances.

| Vessel | ICA | MCA | M1 | M2 | ACoA | M3 | M4 | M5 | M6 |
|---|---|---|---|---|---|---|---|---|---|
| Q, [mm$^3$/s] | 2500 | 1419 | 888 | 543 | 1081 | 531 | 345 | 316 | 227 |
| $R_{peripheral}$, [Pa·s/mm$^3$] | – | – | – | – | 8.99 | 17.3 | 26.3 | 28.6 | 41.4 |

## 6 TREATMENT MODELLING

For a surgical treatment modelling we assume that vessels M3 and M5 were clipped.

To estimate the flow $\tilde{Q}$ through the clipped vessel system the total resistance $\tilde{R}$ of whole system (including visible resistances and peripheral resistances) was computed using (4). The vessels M3 and M5 pass zero flow, therefore the resistance of these vessels is infinity. Knowing the resistance $\tilde{R}$ the flow $\tilde{Q}$ can be calculated as

$$\tilde{Q} = \frac{P_{end} - P_{capillary}}{\tilde{R}}. \quad (9)$$

The pressure in the carotid and capillaries remains unchanged and is 13000 Pa and 3000 Pa respectively. The obtained value of $\tilde{Q}$ is $2.061ml/s$.

Since the clipped geometry cannot be considered as physiological model the formulas (5) are unsuitable for calculating a volumetric flow through each separate vessel at bifurcations. Instead the following formulas may be used:

$$Q_1 = \frac{Q\frac{1}{R_1'}}{\frac{1}{R_1'} + \frac{1}{R_2'}} = \frac{QR_2'}{R_1' + R_2'}, \quad Q_1 = \frac{Q\frac{1}{R_2'}}{\frac{1}{R_1'} + \frac{1}{R_2'}} = \frac{QR_1'}{R_1' + R_2'}, \quad (10)$$

where $R_1'$ and $R_2'$ are total resistances of vessel branches (including visible part and peripheral resistances).

The results of flow computation in the clipped system are in table 5.

Table 5: Volumetric flow through the vessels after surgical treatment and the change of the flow compared to the initial state.

| Vessel | ICA | MCA | M1 | M2 | ACoA | M3 | M4 | M5 | M6 |
|---|---|---|---|---|---|---|---|---|---|
| Q, [mm$^3$/s] | 2061 | 715 | 715 | 287 | 1346 | 0 | 428 | 0 | 287 |
| ΔQ, [mm$^3$/s] | 439 | 704 | 173 | 256 | 265 | 531 | 83 | 316 | 60 |
| Index [%] | 82.4 | 50.4 | 80.5 | 52.9 | 124.5 | 0 | 124.1 | 0 | 126.4 |

Using the obtained flows a numerical modelling run was conducted to calculate pressures in all vessels. The pressure in aneurisms A1 and A2 after the surgical treatment was determined 11831 Pa and 11502 Pa respectively, which is 727 Pa and 1272 Pa higher than before treatment.

## 7 CONCLUSIONS

Mathematical modelling is a powerful tool for blood flow study, prediction and visualisation. Using camera parameters from ANSYS give possibilities to show computational results, such as flow velocities (see figure 7(a)), pressure (fig. 7(b)) and wall shear stress (fig. 7(c)), over the anatomical image of brain vessels. It makes obtained results more clear and intuitive and enhances the quality of surgical treatment planning.

In future work we are going to take into account the elasticity of the vascular wall and to validate obtained results in vitro and in clinical practice.

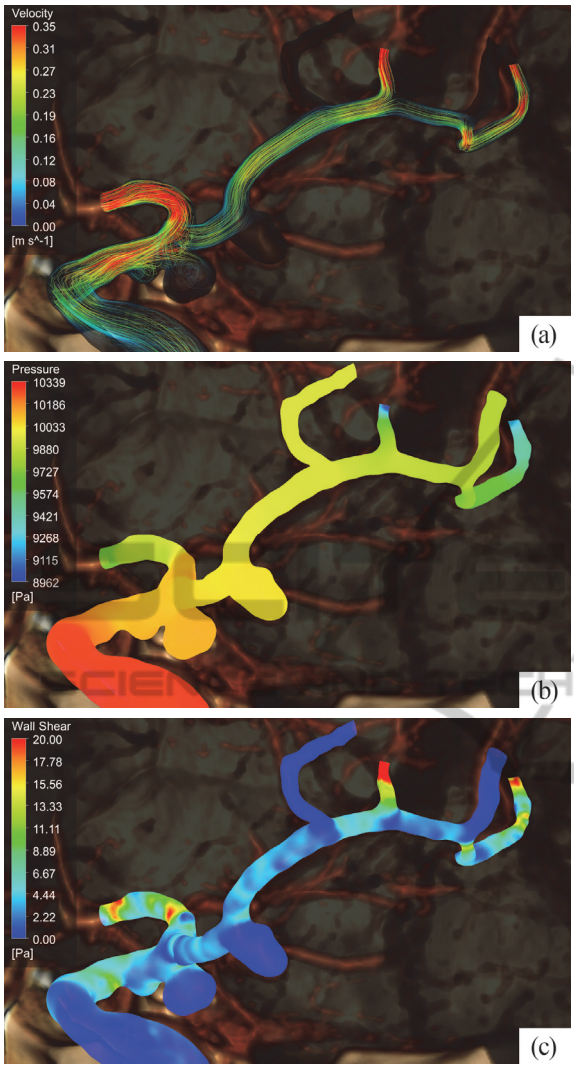


Figure 7: Visualisation of blood flow parameters: (a) flow stream velocity, (b) blood pressure within the vessels, (c) wall shear stress on the vessel boundary.

## REFERENCES


Brown, D., Wang, J., Ho, H., Tullis, S. (2013) 'Numeric Simulation of Fluid–Structure Interaction in the Aortic Arch', *Comp. Biomechanics for Medicine*, pp. 13-23.

Cebral, J.R., Castro, M.A., Soto, O., Löhner R, Alperin N. (2003) 'Blood-flow models of the circle of Willis from magnetic resonance data', *J. of Engineering Mathematics*, vol. 47(3-4), pp. 369–386.

Chupakhin, A.P., Cherevko, A.A. (2012) 'Measurement and Analysis of Local Cerebral Hemodynamics in Patients with Vascular Malformations of the Brain', *Circulation Pathology and Cardiac Surgery,* vol. 4. pp. 27–31. (in Russian).

Kamiya, A., Togawa, T. (1972) 'Optimal branching structure of the vascular tree', *Bull. Math. Biophys,* vol. 34, pp. 431–508.

Kim, H.J., Vignon-Clementel, I.E., Figueroa, C.A., Jansen, K.E., Taylor, C.A. (2010) 'Developing computational methods for three-dimensional finite element simulations of coronary blood flow', *Finite Elements in Analysis and Design*, vol. 46, pp. 514–525.

Krylov, V.V., Gavrilov, A.V., Prirodov, A.B., Grigoryeva, E.V., Ganin, G.V., Arkhipov, I.V., Yatchenko, A.M. (2013a) 'Modeling of hemodynamic changes in the arteries and arterial brain aneurysm in vascular spasm', *Neurosurgery*, vol. 4, pp. 16–25.

Krylov, V., Godkov, I. (2011a) 'Hemodynamic Factors of Formation, Growth and Rupture of Brain Aneurysms', *J. of Neurology,* vol. 1. pp. 4–9. (in Russian).

Krylov, V.V., Godkov, I.M. (2011b) 'Brain Aneurysm Surgery', *Moscow, New Time*. pp. 23–35. (in Russian).

Krylov, V., Lemenev, V., Murashko, A., Luk'yanchikov, V., Dalibaldyan V. (2013b) 'The Treatment of Patients with Atherosclerotic Damage of Brachiocephalic Arteries Combined with Intracranial Aneurysms', *J. of Neurosurgery,* vol. 2. pp. 80–85. (in Russian).

Lorensen, W. E., Cline H.E. (1987) 'Marching Cubes: A high resolution 3D surface construction algorithm', *Computer Graphics*, vol. 21(4), pp. 163–169.

Mittal, N., Zhou, Y., Linares, C., Ung, S., Kaimovitz, B., Molloi, S., Kassab G.S. (2005) 'Analysis of blood flow in the entire coronary arterial tree', *Am. J. Physiol. Heart Circ. Physiol,* vol. 289, pp. H439–H446.

Murray, C.D., (1926a) 'The physiological principle of minimum work. The vascular system and the cost of blood volume', *Natl Acad. Sci. USA* 12, pp. 207–214.

Murray, C.D., (1926b) 'The physiological principle of minimum work applied to the angle of branching of arteries', *J. Gen. Physiol,* vol. 9, pp. 835–841.

Oka, S. (1974) 'Biorheology', *Tokyo: Syokabo*.

Olufsen, M.S., Peskin, C.S., Kim, W.Y., Pedersen, E.M., Nadim, A., Larsen J. (2000) 'Numerical Simulation and Experimental Validation of Blood Flow in Arteries with Structured-Tree Outflow Conditions', *Ann. of Biomed. Eng,* vol. 28(11), pp. 1281–1299.

Rosen, R. (1967) 'Optimality Principles in Biology', *London: Butterworths*.

Sforza, D.M., Putman, Ch. M., Cebral, J.R. (2009) 'Hemodynamics of Cerebral Aneurysms', *Annu Rev. Fluid Mech,* vol. 4. pp. 91–107.

Tateshima, S., Tanishita, K., Omura, H., Villablanca, J.P., Vinuela, F. (2007) 'Intra-Aneurysmal Hemodynamics during the Growth of an Unruptured Aneurysm: In Vitro Study Using Longitudinal CT Angiogram Database', *Am. J. Neuroradiol.* vol. 28, pp.622–627.

Watton, P., Ventikos, Y., Holzapfel, G. (2011) 'Modelling Cerebral Aneurysm Evolution', *Stud. Mechanobiol Tissue Eng. Biomater*, vol. 7, pp. 373–399.

Zamir, M. (1976) 'The role of shear forces in arterial branching', *J. Gen. Biol.* vol. 67, pp. 213–222.

Zamir, M. (1977) 'Shear forces and blood vessel radii in the cardiovascular system', *J. Gen. Physiol.* vol. 69, pp. 449–461.